

Maturation in Action: CryoEM Study of a Viral Capsid Caught during Expansion

David Veesler,^{1,2} Joel Quispe,² Nikolaus Grigorieff,³ Clinton S. Potter,² Bridget Carragher,² and John E. Johnson^{1,*}

¹Department of Molecular Biology

²National Resource for Automated Molecular Microscopy
The Scripps Research Institute, La Jolla, CA 92037, USA

³Rosenstiel Basic Medical Sciences Research Center and Howard Hughes Medical Institute, Brandeis University, Waltham, MA 02454, USA

*Correspondence: jackj@scripps.edu

DOI 10.1016/j.str.2012.05.011

SUMMARY

Bacteriophage HK97 maturation involves discrete intermediate particle forms, comparable to transitional states in protein folding, before reaching its mature form. The process starts by formation of a metastable prohead, poised for exothermic expansion triggered by DNA packaging. During maturation, the capsid subunit transitions from a strained to a canonical tertiary conformation and this has been postulated to be the driving mechanism for initiating expansion via switching hexameric capsomer architecture from skewed to 6-fold symmetric. We report the subnanometer electron-cryomicroscopy reconstruction of the HK97 first expansion intermediate before any crosslink formation. This form displays 6-fold symmetric hexamers, but capsid subunit tertiary structures exhibit distortions comparable to the prohead forms. We propose that coat subunit strain release acts in synergy with the first crosslinks to drive forward maturation. Finally, we speculate that the energetic features of this transition may result from increased stability of intermediates during maturation via enhanced inter-subunit interactions.

INTRODUCTION

Virus maturation corresponds to a transition from an initial noninfectious, often fragile assembly product to an infectious and robust virion (Veesler and Johnson, 2012). Initial subunit interactions occur under conditions where the assembling entities have an association energy that favors assembly over disassembly, but that is near equilibrium to allow “self-correction” of misassembled subunits through annealing (Katen and Zlotnick, 2009). Because viruses require sturdy stability to survive in the extracellular environment, they undergo a staged assembly process due to a mechanochemical reorganization program, encoded in the capsid structure, that governs events underlying maturation.

Assembly and maturation of dsDNA phage capsids are tightly regulated processes, at both the genetic and biochemical levels,

exhibiting conserved features in all *Caudovirales* and in some eukaryotic viruses such as *herpesviruses* (Johnson, 2010; Steven et al., 2005; Veessler and Cambillau, 2011; Veessler and Johnson, 2012). Moreover, the striking conservation of the coat subunit fold observed in all tailed phages and *herpesviruses*, as well as some archeal viruses, suggests that it is derived from a common ancestor preceding the divergence of eukaryotes, bacteria and archea (Baker et al., 2005; Heinemann et al., 2011; Veessler and Cambillau, 2011; Veessler and Johnson, 2012). The lambdoid dsDNA phage HK97 constitutes an accessible model system for studying maturation of such viruses due to its well-characterized genetics and ease of handling. Its capsid maturation pathway involves discrete intermediate particle forms, comparable to transitional states in protein folding, that can be isolated using a combination of molecular biology and biochemical techniques.

The HK97 capsid precursor protein is a fusion of the scaffolding protein (δ -domain, residues 2–103) and of the coat subunit (residues 104–385) that forms a mixture of hexameric and pentameric capsomers upon expression. In vivo, 415 coat subunits (60 hexamers and 11 pentamers) assemble with a dodecameric portal and \sim 60 copies of the viral protease to form the first icosahedral particle termed Prohead-1 (Figure 1). Activation of the viral protease results in digestion of the scaffolding domains and autodigestion to produce small peptide fragments that diffuse out of the particle to yield Prohead-2. The two prohead particle forms exhibit distorted tertiary subunit structures readily recognized by the bent spine helix and the twisted P-domain β sheet. The quaternary structures of these particles also display distortions from canonical symmetry as the hexameric capsomers are skewed, displaying only 2-fold symmetry (Gertsman et al., 2009; Huang et al., 2011). These structural distortions are believed to be induced by the scaffolding domain interactions when capsomers are formed and are stabilized by quaternary interactions following δ -domain proteolysis in Prohead-2 (Gertsman et al., 2010a). Prohead-2 is thus a metastable intermediate trapped in a local free energy minimum that is primed for transition to a lower energy conformation in response to small perturbations. Initiation of dsDNA packaging triggers Prohead-2 expansion, resulting in the formation of successive maturation intermediates (termed expansion intermediates) characterized by an increase of capsid diameter, a reduction of the shell thickness and a “curing” of the hexon asymmetry (Gan et al., 2006; Wikoff et al., 2000). Moreover, H/D exchange experiments coupled to mass spectrometry

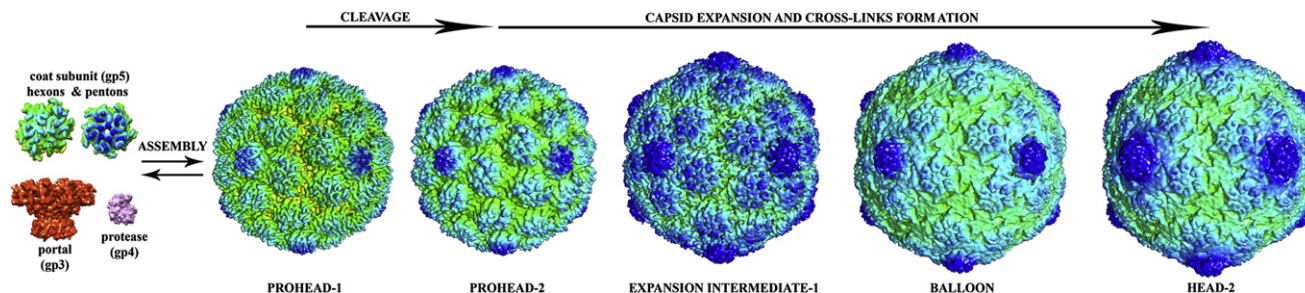


Figure 1. HK97 Assembly and Maturation Pathway

Prohead-1 particles are assembled from 415 copies of the capsid precursor protein, one portal dodecamer, and ~60 copies of the viral protease. Proteolytic processing yields Prohead-2, which is a metastable intermediate, trapped in a local minimum of free energy, primed to transition to a lower energy conformation in response to initiation of DNA packaging. The first expansion intermediate (EI-1) is transient and embodies a significant level of energy in its coat subunit structure that will act in synergy with crosslinking to yield the subsequent expansion intermediates. Biasing of the thermal motions via a Brownian ratchet mechanism based on the capture of coat subunit E-loops at the capsid surface promote switching to the Balloon conformation that will eventually yield the final mature Head-II conformation forming a molecular chainmail stabilized by the presence of 415 covalent crosslinks between coat subunits. All the maps were generated from the maturation intermediate crystal structures and low-pass filtered at 9 Å except for EI-1 where the map corresponds to the cryoEM reconstruction reported in this study and low-pass filtered at 9.3 Å.

(HDXMS) suggested that in intermediates later than the Prohead-2 form, the capsid subunit tertiary structure transitions to a relaxed state similar to those observed in the Balloon and Head-2 crystal structures (Gertsman et al., 2010a, 2010b). The large conformational changes occurring during formation of the first expansion intermediate (EI-1) makes it crosslink competent with isopeptide bonds forming immediately through an autocatalytic mechanism between residues Lys169, on the E-loop of one coat subunit, and Asn356, on the P-domain of an adjacent subunit in a neighboring capsomer (Duda et al., 1995; Popa et al., 1991; Wikoff et al., 2000). Crosslink formation is not concerted, making EI-1 particles transient and the population heterogeneous. Crosslinking promotes formation of the subsequent expansion intermediates and has been proposed to modulate the capsid structural reorganization by biasing thermal motions via a Brownian ratchet mechanism based on the capture of the subunit E-loops (Lee et al., 2008; Ross et al., 2005). The *in vivo* maturation endpoint, Head-2 bears 415 crosslinks with a chainmail topology that dramatically stabilizes the capsid enclosing the genome packaged at near liquid-crystalline density (Helgstrand et al., 2003; Wikoff et al., 2000).

Here, we used an HK97 subunit mutation that prevents formation of crosslink or comparable noncovalent interactions and an expression system that produces virus-like particles indistinguishable from authentic proheads but with the portal replaced by a twelfth coat subunit penton. The mutation stops maturation at the EI-1 intermediate generating a homogeneous population of these particles without E-loop “chainmail” interactions. Comparing these particles with mature Head-2 allows the mechanical role of the Brownian ratchet in maturation to be identified. We determined the subnanometer structure of the crosslink-free EI-1 particle with electron cryomicroscopy (CryoEM) employing single particle protocols. The reconstruction, unexpectedly, reveals that coat subunit monomers exhibit distortions comparable to those observed in the prohead forms although the hexamers are approximately 6-fold symmetric. The observed coat subunit conformations suggest that release of their structural strain adds an energetic assist to crosslinking, driving capsid maturation forward with multiple energetic components. In addition,

the structure suggests that the exothermic nature of capsid maturation (Galisteo and King, 1993) is a consequence of enhanced quaternary interactions that stabilize the downstream intermediates.

RESULTS

CryoEM Reconstruction of the HK97 First Expansion Intermediate: EI-1

A construct encoding an E-loop truncation of the coat subunit was used to produce homogenous virus-like particles stalled at the EI-1 stage of maturation and lacking crosslinks. We carried out an icosahedral reconstruction of this maturation intermediate using 17,116 particle images and single particle techniques. The resulting structure has a resolution of 9.3 Å (Figure S1 available online), exhibits pronounced icosahedral facets and its overall size and morphology are consistent with a previously reported reconstruction obtained at lower resolution (Lee et al., 2008; Ross et al., 2005). The capsid forms a 43 Å thick and 600 Å wide (along 5-fold axes) hollow shell made of 420 coat subunits arranged with a $T = 7$ *laevo* symmetry and with protruding hexamers and pentamers (Figures 2A–2C). The resolution of the reconstruction is qualitatively demonstrated by observed secondary structure elements of the subunits and the straightforward segmentation of individual proteins, either visually or by automated procedures. We further improved the quality of the map by averaging the density of the seven subunits within the icosahedral asymmetric unit.

Architecture of the Coat Subunits

We initially generated an EI-1 pseudo-atomic model by fitting the mature Head-2 X-ray coordinates in the reconstruction because tertiary structure distortion was not anticipated (Gertsman et al., 2009). Previous HDXMS experiments suggested that early HK97 expansion intermediates share the relaxed major capsid protein conformation with the late maturation intermediates as well as with the final Head-2 (Gertsman et al., 2009, 2010a, 2010b; Wikoff et al., 2000). Rigid-body docking of the seven individual subunits forming the icosahedral asymmetric

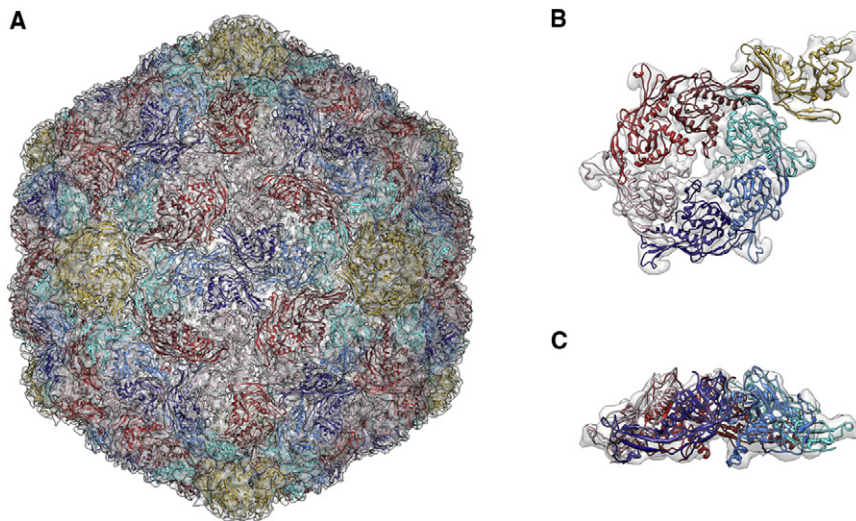


Figure 2. Subnanometer CryoEM Reconstruction of the HK97 First Expansion Intermediate: EI-1

(A) Icosahedrally averaged reconstruction low-pass filtered at 9.3 Å resolution. We generated an EI-1 pseudo-atomic model by rigid-body fitting of the Prohead-II coat subunits (PDB 3E8K) in the map.

(B) The seven subunits forming an icosahedral asymmetric unit are shown fitted in the corresponding 7-fold averaged density viewed from the capsid exterior. The hexon subunits are organized with an approximate 6-fold symmetry.

(C) Side view of the coat subunit hexon depicted in (B). Each of the coat subunits are independently colored.

unit revealed a striking discrepancy between the EM reconstruction and the Head-2 atomic coordinates in the spine helices and the adjacent P-domain β sheets (Figure 3A). As the Prohead-2 coat subunits are characterized by a twisting around the P-domain β sheet along with bending of the spine helix, we used this model to fit into the EI-1 reconstruction. This model dramatically improved the agreement with the density in these regions without compromising agreement with the rest of the density (Figures 3A and 3B). The CryoEM density also shows that the coat protein hexamers are approximately 6-fold symmetric (Figure 1B), in agreement with a previous EI-1 reconstruction (Lee et al., 2008; Ross et al., 2005).

The discrepancy between this EI-1 reconstruction and previous mass spectrometry data can be explained by considering the constructs used to produce the virus-like particles in the two studies (Gertsman et al., 2010a, 2010b). While we used the E-loop deletion mutant to overexpress EI-1 in the current study, the previously characterized “EI-1” harbored a wild-type coat subunit E-loop allowing immediate initiation of cross-link formation. The latter particle form must therefore correspond to EI-2, which is EI-1 with crosslinks but that has not transitioned to the Balloon particle (Lee et al., 2008).

The EI-1 hexons are 140 Å wide and 43 Å thick in our pseudo-atomic model, corresponding to an intermediate configuration between Prohead-2 (123 Å wide and 55 Å thick) and Head-II (157 Å wide and 32 Å thick). The reorganization of the subunits between Prohead-2 and Head-2, from approximately radial to approximately tangential orientation relative to the capsid

surface, is associated with a 2-fold increase in the buried surface area at the interfaces between coat subunits. Accordingly, we observe that the rotation undergone by the subunits to reach the EI-1 state accounts for a substantial portion of the increased buried surface area.

Subunit interactions established at 3-fold and quasi 3-fold axes are known to be unchanged during maturation and to serve as anchoring points allowing preservation of capsid integrity (Gertsman et al., 2009; Wikoff et al., 2000). Although side chain positioning cannot be achieved at the resolution of our reconstruction, our model is fully compatible with retention of the salt bridges established at 3-fold contact points between residues Arg194 and Glu363 as well as between Arg347 and Glu344 (Gertsman et al., 2010a). This observation, along with the observed approximate 6-fold symmetry of the coat subunit hexamers, validates the quality of the pseudo-atomic model and further reinforces the conclusions drawn from it.

Conformation of the Coat Subunit E-Loop

No attempt was made to model the conformation of the E-loop in the previously reported EI-1 studies due to the limited resolution of the reconstructions (Lee et al., 2008; Ross et al., 2005). While in our case the E-loop is absent from the expressed molecule, the density clearly shows the location of the truncated loop and by inference the trajectory of the E-loop, if it were there (Figure 4). They extend toward the capsid exterior, parallel to the spine helix of the neighboring subunit that is within the same hexon or penton, and interact with it though probably less

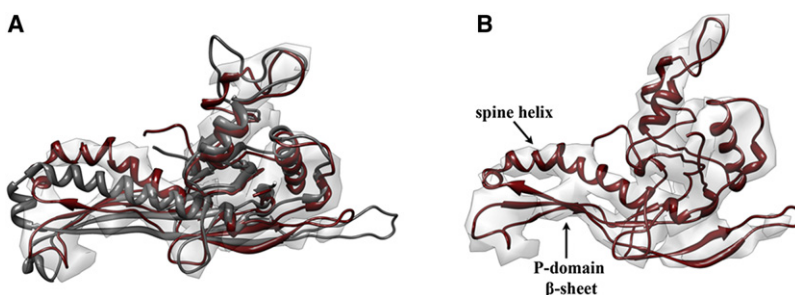


Figure 3. HK97 EI-1 Coat Subunits Are Conformationally Distorted

(A) EI-1 coat subunits exhibit the Prohead-II distorted conformation characterized by twisting around the P-domain β sheet and bending of the spine helix. The Head-II (gray) and Prohead-II (dark red) coat subunits are fitted in the 7-fold averaged EM density to emphasize the conformational strain present in EI-1.

(B) The Prohead-II coat subunit alone is shown within its corresponding density [slightly rotated relative to (A)] to emphasize on the conformational twist around the P-domain β sheet and the spine helix.

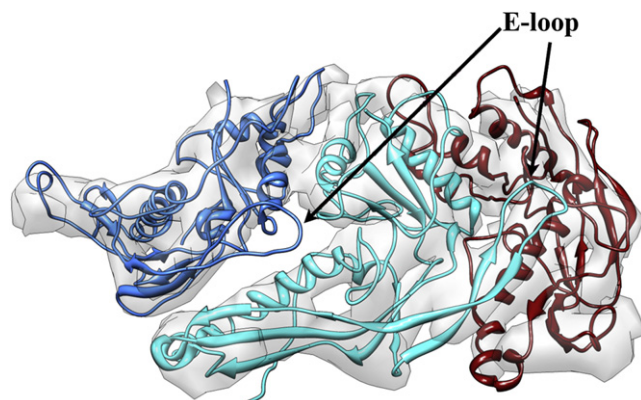


Figure 4. Conformation of the Coat Subunit E-Loops

Semi-tilted view of a coat subunit hexon viewed from the capsid exterior and showing the conformation of the truncated E-loop used in this study to allow trapping the particles at the EI-1 stage. The 7-fold averaged EM density corresponding to three coat subunits is shown along with the fitted atomic coordinates. The E-loops extend toward the capsid exterior and establish contacts (within a given hexon or penton) with the spine helix of the neighboring subunit. These interactions might be involved in maintaining the distorted conformation of the coat subunit at this stage before release in later maturation intermediates to allow crosslink formation.

extensively than in Prohead-2. These interactions may be involved in maintaining the distorted conformation of the coat subunit in EI-1, prior to disengagement as seen in later maturation intermediates. The crosslink formation requires a major repositioning of the E-loop to place the Lys169 side chain near the Gln356 side chain of a subunit belonging to a neighboring capsomer to form the isopeptide bond. As a result, the E-loop conformational change disrupts the intra-capsomeric interactions established with the spine helix probably allowing refolding of the coat subunit to reach its relaxed conformation observed in EI-2 and subsequent particle forms.

DISCUSSION

It was previously suggested that EI-1 represents the maturation ground state and that crosslinking acts via a ratcheting mechanism to shift the global equilibrium toward the Balloon and then the Head-2 forms (Lee et al., 2008; Ross et al., 2005). The results presented here show that EI-1 still embodies a significant degree of conformational strain, due to the bent spine helix and twist of the subunits around the P-domain β sheet. The structure implies that the transition to the relaxed coat subunit conformation is tightly correlated with formation of the first crosslinks and/or non-covalent quaternary interactions established by the tip of the E-loops. Indeed, the ability to arrest maturation at the EI-1 stage constituted a unique opportunity to demonstrate that in the absence of crosslinks or such non-covalent E-loop interactions the capsid still resides in a stressed conformation harboring distorted coat subunits despite the formation of ~ 6 -fold symmetric hexamers. The observation that expansion can be induced by various physico-chemical stimuli (such as pH change or iso-butanol) and the characteristic two-state transition between Prohead-2 and EI-1 evidenced by SAXS measurements indicate that the latter has a lower energy than its precursor

Table 1. Residues Involved in Coat Subunit Contacts during Maturation

Residue	Prohead-II	Head-II
Hydrophobic (number, % of contact residues)	197 (38)	571 (51)
Polar/charged (number, % of contact residues)	322 (62)	557 (49)

(Gertsman et al., 2010b; Lee et al., 2005). However, our results indicate that EI-1 is still storing energy in its structure, probably to ensure that, in combination with formation of the first crosslinks, the maturation moves forward (Figure 1) and reaches the EI-2 particle form (with numerous crosslinks and coat subunits with canonical tertiary structure). Disruption of the spine helix/E-loop interactions facilitates Brownian motion-mediated sampling of the conformational space by uncrosslinked E-loops and formation of additional crosslinks between capsomers, making the maturation process irreversible. It should be noted that expansion from Prohead-2 to EI-1 results in a $\sim 10\%$ increase in particle dimension but further expansion does not occur in the overall particle dimensions until 60% of the crosslinks are formed. When the expansion occurs from EI-1 to the Balloon it is also a two-state transition with no detectable intermediates as demonstrated by time-resolved SAXS experiments (Lee et al., 2008).

Differential scanning calorimetry (DSC) studies of bacteriophage P22 maturation revealed that its expansion is strongly exothermic (Galisteo and King, 1993). The striking conservation of the coat subunit fold among tailed phages as well as of many aspects of their maturation suggests that exothermic expansion is a common feature of such viruses (Johnson, 2010; Veessler and Cambillau, 2011; Veessler and Johnson, 2012). During expansion, coat subunits establish an increasing number of interactions with each other to stabilize the capsid concomitantly with dsDNA packaging in order to withstand the remarkable pressure generated by the genome (Fuller et al., 2007; Veessler and Johnson, 2012). The gradual enhancement of subunit intertwining increases by a factor ~ 2 the total buried surface area involving the subunits from a given icosahedral asymmetric unit as well as the number of residues participating to these contacts during the transition from Prohead-2 to Head-2. During this transition both hydrophobic and polar interactions are increased, but the proportions of each of these are dramatically modified in favor of hydrophobic stabilization (Table 1). However, electrostatic complementarity of the coat subunit A domains seems to play a major role in the reorganization observed. In the skewed Prohead-2 hexamers, subunits B and E adopt a specific conformation involving only tenuous interactions of their A-domains with the anticlockwise located neighboring subunits (view from the capsid exterior) in comparison to the other four subunits (Figures 5A–5F). In contrast, all the Head-2 hexamer subunits are characterized by the formation of identical interactions locking the capsomer conformation by the high level of A-domain charge complementarity (Figures 5G–5J). Polar and covalent interactions create thus specific contacts and provide the directionality for rearranging subunit-subunit interactions. It is worth mentioning that release of the strain in coat subunit pentamers during expansion provokes a dramatic reorganization of the hexamers/pentamers interactions. Therefore, the energetically unfavorable coat subunit refolding event occurring during capsid

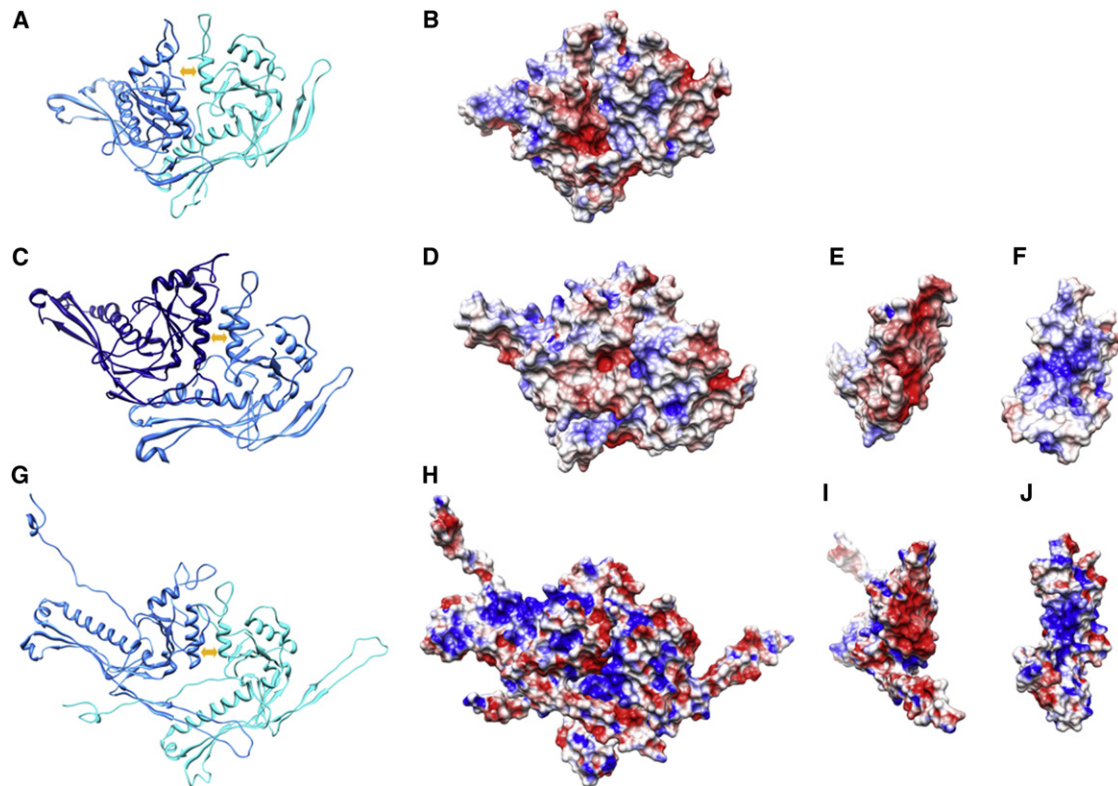


Figure 5. Reorganization of Coat Subunit Interfaces During Maturation

(A and B) Ribbon (A) and electrostatic surface potential (B) rendering of the Prohead-2 A/B dimer. Subunit B exposes a negatively charged patch of residues from its A domain toward the capsid exterior (the situation is identical at the interface between subunits D and E) that will be engaged in interactions with subunit A at a later stage of maturation (cf. panels G–J).

(C and D) Ribbon (C) and electrostatic surface potential (D) rendering of the Prohead-2 B/C dimer in which the two monomers are optimally aligned relative to each other to maximize interactions of their A-domains.

(E and F) Subunits B (E) and C (F) are shown individually after rotation to reveal the nature of the interacting surfaces.

(G and H) Ribbon (G) and electrostatic surface potential (H) rendering of the Head-2 A/B dimer.

(I and J) Subunits A (I) and B (J) are shown individually after rotation to reveal the nature of the interacting surfaces. The orange arrows indicate the interacting surface area between A-domains in the different ribbon rendering.

expansion is likely compensated by the enthalpy gain from the increase in polar interactions and by enhancement of hydrophobic interactions in addition to the contribution of chainmail crosslinks. This drives the maturation process forward, ensuring its irreversibility (beyond the EI-1 stage) by a progressive stabilization of the different expansion intermediates likely explaining the exothermic nature of bacteriophage expansion. Work is still in progress to address the discrepancy between the EM and SAXS data discussed here and some previously reported DSC results (Ross et al., 2005; 2006).

Overall, the program encoded in the initial assembly products that directs particle maturation to the fully mature particle, is slowly being discerned as a remarkable integration of chemistry, thermodynamics, and mechanobiology that evolution has tuned to a very high level.

EXPERIMENTAL PROCEDURES

Preparation of EI-1

We used a mutated version of the HK97 gp5 coat subunit in which residues 159–171 are replaced with residues APGD (Gertsman et al., 2009). This

construct harbors an E-loop shortened at its distal part preventing the formation of crosslinks and of part of the quaternary interactions. The capsid protein (gp5) and the protease (gp4) were coexpressed using *Escherichia coli* BL21pLysS cells induced with 0.4 mM IPTG at 28°C overnight. After harvesting, cells were lysed using the Bugbuster reagent (Merck) supplemented with 20 µg/ml of DNase I and 10 mM MgSO₄. Cell debris were removed by centrifugation and capsids were precipitated in presence of 0.5 M NaCl and 6% polyethylene glycol 8000. Remaining Prohead-1 particles were disassembled by incubation in 2M KCl, 100 mM CHES, pH 9.5 for 5–6 hr before purification on a 10%–30% glycerol gradient. Prohead-2 expansion was triggered by incubation in a buffer Na-acetate pH4.0, 300 mM NaCl during 6 hr at RT. The pH was raised to 7.5 and an anion exchange chromatography (5 ml FF DEAE) was carried out before exchanging the buffer of the particles by ultracentrifugation to 10 mM Tris pH7.5, 40 mM NaCl.

Data Collection

Purified EI-1 capsids were prepared for cryoEM analysis by placing 3 µl of sample on a C-flat carbon-coated grids (Protochips, Inc.) previously glow-discharged in a Solarus plasma cleaner (Gatan, Inc.). Grids were manually blotted before plunging into liquid ethane and subsequently transferred to liquid nitrogen in which they were stored. Data were acquired on a Tecnai F20 Twin transmission electron microscope operated at 200 keV, using a dose of 20 e-/Å², a nominal magnification of 62,000 and a nominal

underfocus ranging from 1.0 to 3.5 μm . One data set containing 1,714 images was automatically collected using the Legion data collection software (Suloway et al., 2005) using a Tietz F415 4K x 4K pixel CCD camera (15 μm pixel).

Data Processing

We extensively relied on the Appion processing pipeline for initial processing of the images (Lander et al., 2009). The contrast transfer function for each micrograph was estimated using CTFind3 and applied to each micrograph before particle extraction (Mindell and Grigorieff, 2003). We manually masked all the micrographs to exclude the particles lying on the carbon regions before carrying out an automated particle picking using FindEM (Roseman, 2004). Capsids were extracted using a box size of 704 pixels and binned by a factor of 2 for processing yielding a stack of 24,394 particles. Three-dimensional reconstruction was performed using FREALIGN (Grigorieff, 2007) including 17,116 particle images and an initial model obtained by low-pass filtering at 50 \AA the EI-2 pseudo-atomic model previously reported (Lee et al., 2008). The resolution of 9.3 \AA for the EI-1 reconstruction was assessed by calculating the Fourier shell correlation at a cutoff of 0.143 (Grigorieff and Harrison, 2011). The amplitudes of the resulting refined structure were adjusted with the SPIDER software package to more closely resemble those of an experimental low-angle X-ray scattering data (Frank et al., 1996; Gabashvili et al., 2000). Averaging of the seven subunits belonging to the icosahedral asymmetric unit has been carried out using the RAVE package (LSQMAN, MAMA, IMP, and AVE) (Kleywegt et al., 2001).

Structure Analysis

We generated a pseudo-atomic model of the EI-1 capsid by rigid-body fitting the Prohead-2 atomic coordinates (PDB 3E8K) in the reconstruction using UCSF Chimera (Goddard et al., 2007) before carrying out an energy minimization imposing strict icosahedral symmetry with CNS 1.3 (Brunger, 2007; Brünger et al., 1998). Visualization was carried out with Coot (Emsley et al., 2010). Interface and interaction analyses were done using ViperDB (Carrillo-Tripp et al., 2009). Electrostatic surface potential calculations were done using pdb2pqr (Dolinsky et al., 2004) and APBS (Baker et al., 2001).

ACCESSION NUMBERS

The accession number for the EI-1 cryoEM map reported in this paper is EMD-2112.

SUPPLEMENTAL INFORMATION

Supplemental Information includes one figure and can be found with this article online at [doi:10.1016/j.str.2012.05.011](https://doi.org/10.1016/j.str.2012.05.011).

ACKNOWLEDGMENTS

We thank Andrew Routh for critical reading of the manuscript. This project was supported by grants from the NIH (R01 AI040101), NCR (2P41RR017573-11), and the NIGMS (9 P41 GM103310-11) as well as a FP7 Marie-Curie IOF fellowship (273427) attributed to D.V. Molecular graphics and analyses were performed with the UCSF Chimera package. Chimera is developed by the Resource for Biocomputing, Visualization, and Informatics at the University of California, San Francisco, with support from the National Institutes of Health (National Center for Research Resources grant 2P41RR001081 and National Institute of General Medical Sciences grant 9P41GM103311).

Received: April 15, 2012

Revised: May 20, 2012

Accepted: May 21, 2012

Published online: June 28, 2012

REFERENCES

Baker, N.A., Sept, D., Joseph, S., Holst, M.J., and McCammon, J.A. (2001). Electrostatics of nanosystems: application to microtubules and the ribosome. *Proc. Natl. Acad. Sci. USA* 98, 10037–10041.

Baker, M.L., Jiang, W., Rixon, F.J., and Chiu, W. (2005). Common ancestry of herpesviruses and tailed DNA bacteriophages. *J. Virol.* 79, 14967–14970.

Brunger, A.T. (2007). Version 1.2 of the Crystallography and NMR system. *Nat. Protoc.* 2, 2728–2733.

Brünger, A.T., Adams, P.D., Clore, G.M., DeLano, W.L., Gros, P., Grosse-Kunstleve, R.W., Jiang, J.S., Kuszewski, J., Nilges, M., Pannu, N.S., et al. (1998). Crystallography & NMR system: A new software suite for macromolecular structure determination. *Acta Crystallogr. D Biol. Crystallogr.* 54, 905–921.

Carrillo-Tripp, M., Shepherd, C.M., Borelli, I.A., Venkataraman, S., Lander, G., Natarajan, P., Johnson, J.E., Brooks, C.L., 3rd, and Reddy, V.S. (2009). VIPERdb2: an enhanced and web API enabled relational database for structural virology. *Nucleic Acids Res.* 37 (Database issue), D436–D442.

Dolinsky, T.J., Nielsen, J.E., McCammon, J.A., and Baker, N.A. (2004). PDB2PQR: an automated pipeline for the setup of Poisson-Boltzmann electrostatics calculations. *Nucleic Acids Res.* 32 (Web Server issue), W665–67.

Duda, R.L., Hempel, J., Michel, H., Shabanowitz, J., Hunt, D., and Hendrix, R.W. (1995). Structural transitions during bacteriophage HK97 head assembly. *J. Mol. Biol.* 247, 618–635.

Emsley, P., Lohkamp, B., Scott, W.G., and Cowtan, K. (2010). Features and development of Coot. *Acta Crystallogr. D Biol. Crystallogr.* 66, 486–501.

Frank, J., Radermacher, M., Penczek, P., Zhu, J., Li, Y., Ladjadi, M., and Leith, A. (1996). SPIDER and WEB: processing and visualization of images in 3D electron microscopy and related fields. *J. Struct. Biol.* 116, 190–199.

Fuller, D.N., Raymer, D.M., Rickgauer, J.P., Robertson, R.M., Catalano, C.E., Anderson, D.L., Grimes, S., and Smith, D.E. (2007). Measurements of single DNA molecule packaging dynamics in bacteriophage lambda reveal high forces, high motor processivity, and capsid transformations. *J. Mol. Biol.* 373, 1113–1122.

Gabashvili, I.S., Agrawal, R.K., Spahn, C.M., Grassucci, R.A., Svergun, D.I., Frank, J., and Penczek, P. (2000). Solution structure of the E. coli 70S ribosome at 11.5 \AA resolution. *Cell* 100, 537–549.

Galisteo, M.L., and King, J. (1993). Conformational transformations in the protein lattice of phage P22 procapsids. *Biophys. J.* 65, 227–235.

Gan, L., Speir, J.A., Conway, J.F., Lander, G., Cheng, N., Firek, B.A., Hendrix, R.W., Duda, R.L., Liljas, L., and Johnson, J.E. (2006). Capsid conformational sampling in HK97 maturation visualized by X-ray crystallography and cryo-EM. *Structure* 14, 1655–1665.

Gertsman, I., Gan, L., Guttman, M., Lee, K., Speir, J.A., Duda, R.L., Hendrix, R.W., Komives, E.A., and Johnson, J.E. (2009). An unexpected twist in viral capsid maturation. *Nature* 458, 646–650.

Gertsman, I., Fu, C.Y., Huang, R., Komives, E.A., and Johnson, J.E. (2010a). Critical salt bridges guide capsid assembly, stability, and maturation behavior in bacteriophage HK97. *Mol. Cell. Proteomics* 9, 1752–1763.

Gertsman, I., Komives, E.A., and Johnson, J.E. (2010b). HK97 maturation studied by crystallography and H₂O exchange reveals the structural basis for exothermic particle transitions. *J. Mol. Biol.* 397, 560–574.

Goddard, T.D., Huang, C.C., and Ferrin, T.E. (2007). Visualizing density maps with UCSF Chimera. *J. Struct. Biol.* 157, 281–287.

Grigorieff, N. (2007). FREALIGN: high-resolution refinement of single particle structures. *J. Struct. Biol.* 157, 117–125.

Grigorieff, N., and Harrison, S.C. (2011). Near-atomic resolution reconstructions of icosahedral viruses from electron cryo-microscopy. *Curr. Opin. Struct. Biol.* 21, 265–273.

Heinemann, J., Maaty, W.S., Gauss, G.H., Akkadevi, N., Brumfield, S.K., Rayaprolu, V., Young, M.J., Lawrence, C.M., and Bothner, B. (2011). Fossil record of an archaeal HK97-like provirus. *Virology* 417, 362–368.

Helgstrand, C., Wikoff, W.R., Duda, R.L., Hendrix, R.W., Johnson, J.E., and Liljas, L. (2003). The refined structure of a protein catenane: the HK97 bacteriophage capsid at 3.44 \AA resolution. *J. Mol. Biol.* 334, 885–899.

Huang, R.K., Khayat, R., Lee, K.K., Gertsman, I., Duda, R.L., Hendrix, R.W., and Johnson, J.E. (2011). The Prohead-I structure of bacteriophage HK97: implications for scaffold-mediated control of particle assembly and maturation. *J. Mol. Biol.* 408, 541–554.

- Johnson, J.E. (2010). Virus particle maturation: insights into elegantly programmed nanomachines. *Curr. Opin. Struct. Biol.* *20*, 210–216.
- Katen, S., and Zlotnick, A. (2009). The thermodynamics of virus capsid assembly. *Methods Enzymol.* *455*, 395–417.
- Kleywegt, G.J., Zou, J.Y., Kjeldgaard, M., and Jones, T.A. (2001). Crystallography of biological macromolecules. In *International Tables for Crystallography, Volume F*, M.G. Rossmann and E. Arnold, eds. (Hoboken, NJ: Wiley), pp. 353–356, 366–367.
- Lander, G.C., Stagg, S.M., Voss, N.R., Cheng, A., Fellmann, D., Pulokas, J., Yoshioka, C., Irving, C., Mulder, A., Lau, P.W., et al. (2009). Appion: an integrated, database-driven pipeline to facilitate EM image processing. *J. Struct. Biol.* *166*, 95–102.
- Lee, K.K., Tsuruta, H., Hendrix, R.W., Duda, R.L., and Johnson, J.E. (2005). Cooperative reorganization of a 420 subunit virus capsid. *J. Mol. Biol.* *352*, 723–735.
- Lee, K.K., Gan, L., Tsuruta, H., Moyer, C., Conway, J.F., Duda, R.L., Hendrix, R.W., Steven, A.C., and Johnson, J.E. (2008). Virus capsid expansion driven by the capture of mobile surface loops. *Structure* *16*, 1491–1502.
- Mindell, J.A., and Grigorieff, N. (2003). Accurate determination of local defocus and specimen tilt in electron microscopy. *J. Struct. Biol.* *142*, 334–347.
- Popa, M.P., McKelvey, T.A., Hempel, J., and Hendrix, R.W. (1991). Bacteriophage HK97 structure: wholesale covalent cross-linking between the major head shell subunits. *J. Virol.* *65*, 3227–3237.
- Roseman, A.M. (2004). FindEM—a fast, efficient program for automatic selection of particles from electron micrographs. *J. Struct. Biol.* *145*, 91–99.
- Ross, P.D., Cheng, N., Conway, J.F., Firek, B.A., Hendrix, R.W., Duda, R.L., and Steven, A.C. (2005). Crosslinking renders bacteriophage HK97 capsid maturation irreversible and effects an essential stabilization. *EMBO J.* *24*, 1352–1363.
- Ross, P.D., Conway, J.F., Cheng, N., Dierkes, L., Firek, B.A., Hendrix, R.W., Steven, A.C., and Duda, R.L. (2006). A free energy cascade with locks drives assembly and maturation of bacteriophage HK97 capsid. *J. Mol. Biol.* *364*, 512–525.
- Steven, A.C., Heymann, J.B., Cheng, N., Trus, B.L., and Conway, J.F. (2005). Virus maturation: dynamics and mechanism of a stabilizing structural transition that leads to infectivity. *Curr. Opin. Struct. Biol.* *15*, 227–236.
- Suloway, C., Pulokas, J., Fellmann, D., Cheng, A., Guerra, F., Quispe, J., Stagg, S., Potter, C.S., and Carragher, B. (2005). Automated molecular microscopy: the new Legimon system. *J. Struct. Biol.* *151*, 41–60.
- Veesler, D., and Cambillau, C. (2011). A common evolutionary origin for tailed-bacteriophage functional modules and bacterial machineries. *Microbiol. Mol. Biol. Rev.* *75*, 423–433.
- Veesler, D., and Johnson, J.E. (2012). Virus maturation. *Annual Rev. Biophys.* *41*, 473–496.
- Wikoff, W.R., Lijas, L., Duda, R.L., Tsuruta, H., Hendrix, R.W., and Johnson, J.E. (2000). Topologically linked protein rings in the bacteriophage HK97 capsid. *Science* *289*, 2129–2133.

Structure, Volume 20

Supplemental Information

Maturation in Action: CryoEM Study

of a Viral Capsid Caught during Expansion

David Veesler, Joel Quispe, Nikolaus Grigorieff, Clinton S. Potter, Bridget Carragher, and John E. Johnson

Inventory of Supplemental Information

Supplementary Figure 1. Fourier Shell Correlation of the HK97 EI-1 reconstruction

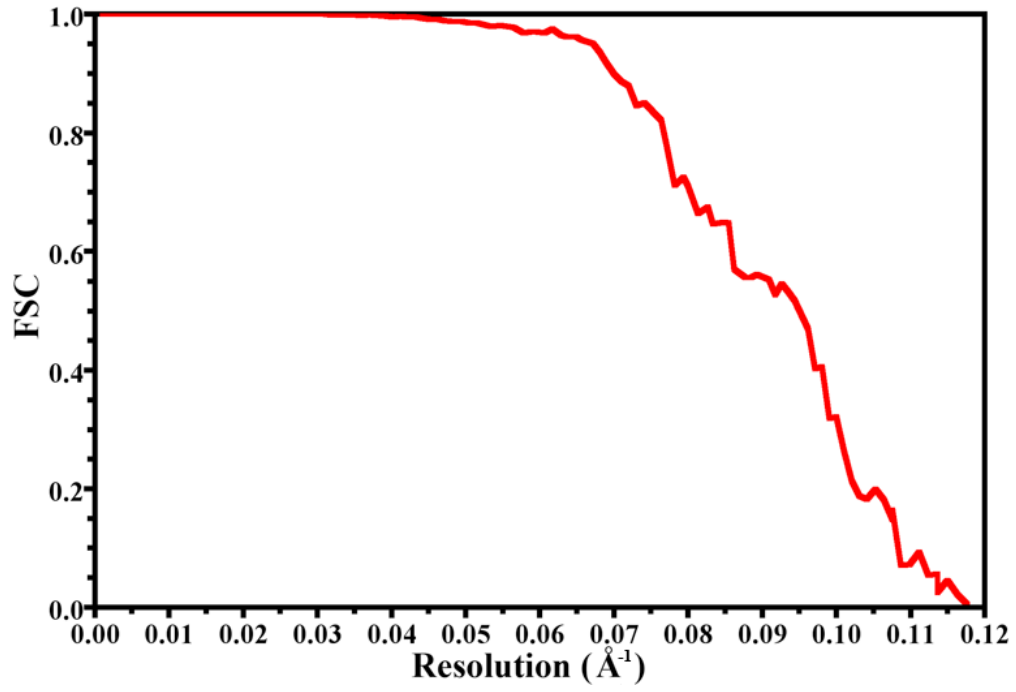


Figure S1. Fourier Shell Correlation of the HK97 EI-1 reconstruction. The resolution is estimated to be 9.3 Å at FSC=0.143.